Fast mosaicking method of InSAR-generated multi-stripe digital elevation model

HONG Zhong-Hua[1],　SUN Peng-Fei[1],　ZHOU Ru-Yan[1],　TONG Xiao-Hua[2*],　FENG Yong-Jiu[2],　LIU Shi-Jie[2]

（1. The College of Information Technology, Shanghai Ocean University, Shanghai 201306, China；
2. College of Surveying and Geo−Informatics, Tongji University, Shanghai 200092, China）

Abstract：A large-scale rapid DEM mosaicking method was proposed. In this method, dense tie-points were extracted from the DEM overlap areas using a block matching strategy, and the systematic errors of plane and elevation were corrected through block adjustment. Thus, an entire DEM set was generated using the mosaicking strategy of first along-track followed by cross-track. A computing strategy was adopted to accelerate the processing speed to improve the efficiency of the entire mosaicking process. The experimental results showed that the CPU/GPU asynchronous parallel method proposed in this study improves the processing efficiency by more than 18 times that of a single CPU, and realises the seamless mosaicking of multi-stripe DEMs.

Key words：DEM, tie-points, block adjustment, mosaicking, accelerate

PACS: 07. 07. Df, 84. 40. Xb

InSAR 生成 DEM 的多条带快速融合方法

洪中华[1],　孙鹏飞[1],　周汝雁[1],　童小华[2*],　冯永玖[2],　刘世杰[2]
（1. 上海海洋大学 信息学院，上海 201306；
2. 同济大学 测绘与地理信息学院，上海 200092）

摘要：提出了一种 DEM 大范围快速融合方法，该方法首先 DEM 重叠区域通过分块匹配策略提取密集连接点并进行区域网平差修正平面和高程上的系统误差；在此基础上通过先顺轨后垂轨的策略融合生成一整副 DEM；同时为了提升整个融合效率，采用策略加快处理速度。实验结果表明，提出 CPU/GPU 异步并行方法比单 CPU 处理效率提升了 18 倍，实现了多条带 DEM 无缝融合。

关　键　词：DEM；连接点；区域网平差；融合；加速

中图分类号：TP79　　**文献标识码**：A

Introduction

Interferometry synthetic aperture radar（InSAR）is the combination of the radio astronomical interference technology and SAR remote sensing technology. The InSAR technology has been widely used in the production and updating of global high-precision digital elevation model（DEM）products [1-2]. The DEM is a digital representation of cartographic information in grid form. As the most basic product in the surveying and mapping geographic information industry, DEM has been widely applied in ecology, agriculture, hydrological modelling, and other scientific fields because of its simple data structure and wide availability [3-5].

There is little variation in the DEM errors of the same stripe generated by InSAR technology. Owing to the difference in systematic error for the different stripes, there may be some situations such as the opposite error sign, which leads to the relative error between DEMs. In practice, the systematic error source of the overlapping area not only has an elevation error, but also a plane positioning error [6]. To better analyse the information and obtain a large-scale DEM, the DEMs need to be unified into the same benchmark. Registration between DEMs is

key and DEMs are corrected using block adjustment. The DEM matching should be performed to first obtain the transformation relationship between the DEMs in the process of block adjustment. Multiple adjacent orbit DEMs are then fused together through various interpolation algorithms to obtain a high-quality DEM with uniform error characteristics [7].

Tie-points are extracted for the appropriate DEM calibration steps. Huber et al. used the central point of the 1 × 1 km chip in the overlap area of adjacent DEMs as the tie-point [8], but the error of the tie-point was large. In the process of block adjustment, Gonzalez et al. calibrated and adjusted all DEMs with ground control points (GCPs) [9], and Gruber et al. used the least squares method for block adjustment [10]. Elmiro et al. used laser measurement data (ICESat/GLAS) to replace traditional control points to correct the DEM error [11]. Jain et al. adopted a simple and average stitching method for DEM mosaicking [12], and there were obvious seams at the edge of the overlapping area. Among mosaic methods in the field of image processing, the feathering-based method is considered to be the best [13]; although the performance is satisfactory for two DEMs, it cannot achieve seamless mosaicking for multi-stripe DEM processing. Uss et al. proposed a no-reference method to estimate DEM vertical error parameters [14]. But the modified method could not estimate the plane positioning error parameters. Deng et al. proposed a methodology based on 3D point clouds rather than using a raster format [15]. However, iterative closest point (ICP) algorithm had great dependence on the changing initial value. And it was easy to fall into the local optimal solution. Rajeshreddy et al. proposed a novel framework using a hybrid method based on feathering to arrange DEM scenes and mosaic DEM [16]. The elevation values in the overlapping regions had a smooth transition. But the method had a limitation in mosaicking DEM with large systematic error in overlapping area.

The challenge of extended time requirements remains in existing large-scale multi-stripe DEM mosaicking methods. To overcome the limitation of poor processing time, a fast large-scale DEM mosaicking method based on the CPU/GPU asynchronous parallel construct was proposed, and the experiment was conducted on the TanDEM-X dataset. The experimental results showed that the efficiency of the mosaicking method proposed in this study is improved by more than 10 times, and seamless mosaicking was evaluated.

The remainder of this paper is organised as follows. Section 1 describes the large-scale multi-stripe DEM mosaicking method. Section 2 introduces the CPU/GPU parallel computing strategy. Section 3 verifies the effectiveness of the algorithm through experiments and presents the research results. Finally, conclusions are presented in Section 4.

1 Large-scale multi-stripe DEM mosaicking method

The DEM error correction process depends on DEM geocoding, especially located in overlapping areas of the adjacent DEM. The two important steps primary affecting the output DEM mosaicking quality are registration and mosaicking [13]. Combined with the extracted dense tie-points and laser control points, the plane and elevation systematic errors of the InSAR-generated DEM can be corrected through the block adjustment step, ensuring the geometric continuity of the DEM. The DEM mosaicking sequence in the given region of interest was compiled according to the along-track and cross-track directions. The DEMs in the same along-track direction were fused first and then fused in the cross-track direction. The large-scale multi-stripe DEM mosaicking method is shown in Fig. 1.
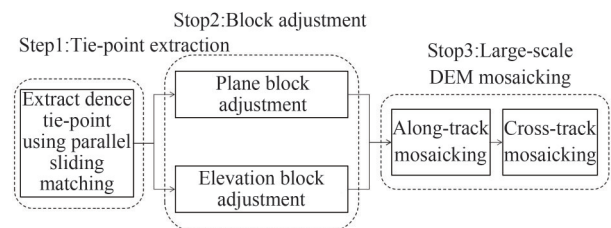
Fig. 1 Large-scale multi-stripe digital elevation model (DEM) mosaicking method
图1 大范围多条带DEM融合方法处理流程

1.1 Dense tie-point extraction

The tie-point, as the input of the DEM block adjustment, is located in the overlapping area of the adjacent DEMs. Because noise degrades the quality of each DEM toward the edge, the tie-point should be located in the centre of the overlap area. Owing to different DEM parameter corrections, some initial positioning errors of the DEM are large. In this study, a matching strategy from rough to fine was adopted to obtain accurate coordinates of the tie-point. Among them, the normalised cross correlation function is used for rough matching because it has good noise resistance. In the process of rough matching, down sampling TanDEM, having the same resolution as SRTM DEM, is registered to the Shuttle Radar Topography Mission (SRTM) over a larger range. And positioning errors between TanDEM can be effectively controlled within a small range. The next fine matching can better extract high-precision tie-points. In the fine matching process, the position of the overlapping area was determined, and the centre of the overlapping region was calculated in advance. The uniformly-spaced tie-point coordinates was calculated using the information. The extraction of high-precision tie-points can be used for DEM error correction. In this study, a dense tie-point extraction method was adopted to obtain precise high-precision tie-points. High-precision tie-points can improve the accuracy of multi-stripe DEM error correction. The process of efficient tie-point extraction is illustrated in Fig. 2.

The DEM features include elevation, slope, and texture, among which elevation information is the most direct display of DEM topographic information. In the overlap area, the chips were divided according to a cer-
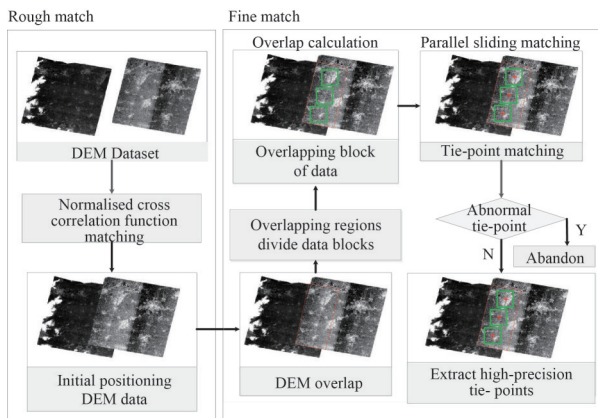
Fig. 2　Processing flow of digital elevation model（DEM）multi-stripe matching

图2　DEM多条带匹配处理流程

tain interval and size. The chips were divided into square areas within the overlap area, and the sliding matching region was the square area set by the data parameters. The tie-point extraction method using an area-based matching approach was adopted to register the chips in the adjacent DEM as shown in Fig. 3.
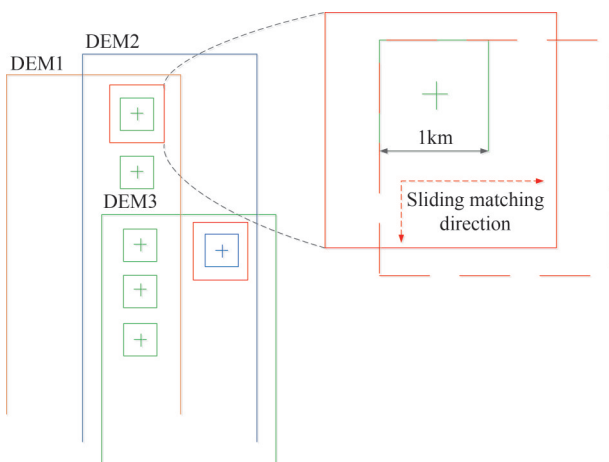
Fig. 3　Chips partition and sliding matching

图3　数据块划分及滑动匹配

In the process of loading DEM data, the ignored value of the data is loaded at the same time. To avoid affecting the accuracy of the extraction tie-point, this study assessed the validity of the data chip elevation data before tie-point matching. The positioning errors of the two data chips were corrected by sliding matching of the data chips in the overlap area. The matching measure function adopted a relatively robust and efficient standard deviation of the elevation difference and is described in Eq. 1.

$$R(i,j) = \sqrt{\frac{1}{w*h} \sum_{w,h} \{[T(x,y) - I(x',y')] - u\}^2} , (1)$$

where the original data chip is denoted as I, the data chip to be matched is T, the average value of the elevation difference between I and T is u, and represents the

pixel of the data chip, (i,j) is the sliding position of the data chip, and w and h are the width and height of the data chip to be matched, respectively.

To further improve the accuracy of the extraction tie-point, the fitting surface minimum of the adjacent eight pixels corresponding to the data chip elevation difference standard deviation, and bilinear interpolation is performed to obtain the elevation value of the sub-pixel coordinate tie-point. The affine model was constructed using the obtained pairs of tie-points, and the outliers were screened with the root mean square error to obtain high-precision pairs of tie-points.

1. 2　DEM block adjustment

The elevation error of the DEM adjustment method trajectory system is used to meet the required elevation accuracy for the quality evaluation of tie-point extraction, in addition to the visual interpretation method. Using the plane constraint of the tie-point and the elevation constraint of the elevation control point, plane block adjustment and elevation block adjustment are performed, respectively.

1. 2. 1　Plane block adjustment

The geographic coordinates of each pixel are determined by the geodetic coordinates of the corner points according to the pixel resolution, and its model is shown in Eqs.2−3.

$$X = a_{11}x + a_{12}y + dx \qquad , (2)$$

$$Y = a_{21}x + a_{22}y + dy \qquad . (3)$$

The plane coordinates of each DEM were adjusted according to the six-parameter affine transformation model. (x, y) are the coordinates of the tie-point. Taking the pair of tie-points matched by two stripes DEM as an example, stripe J is the matching DEM, stripe K is the reference DEM, and constraints are generated through the consistency of geographic coordinates of the tie-points. The matrix form of the error equation is obtained, and the coefficient of error correction model is obtained using the least squares principle to eliminate the plane coordinate system error of each DEM.

1. 2. 2　Elevation block adjustment

The objective of DEM block adjustment is to estimate the elevation error of the system to meet the required elevation accuracy. The elevation system error mainly has vertical displacement and inclination, and the systematic error can be approximated by a third-order polynomial. The error correction model for elevation adjustment is introduced in Eq. 4.

$$g(x_i,y_i) = a_0 + a_1x_i + a_2x_i^2 + a_3x_i^3 + b_1y_i + k \cdot x_i \cdot y_i, (4)$$

where $g(x, y)$ is the elevation error correction equation of the stripe, and (x, y) are the coordinates of the tie-points or GCPs.

After the matrix form of the error equation is obtained, the coefficient of error correction model can be obtained using the least squares principle, and the systematic error of the elevation direction of each DEM can be eliminated.

1. 3　DEM mosaicking

After correcting the systematic errors of plane and

elevation through block adjustment, the adjacent DEM generated by InSAR, especially in the overlapping area of the DEM, ensures continuity in the plane and elevation directions. According to the orbital direction of the satellite image, the multi-stripe DEMs in the given region of interest are first fused one by one in the along-track direction. The large-scale along-track DEMs are fused one by one in the cross-track direction. Finally, as shown in Fig. 6, a whole set of large-scale DEMs is seamlessly fused.
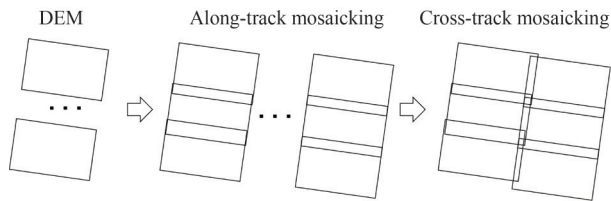
Fig. 6　Schematic diagram of digital elevation model（DEM）mosaicking strategy
图6　DEM融合策略示意图

The feathering-based mosaicking method determines the weight value of the mosaicking elevation based on the distance from the cell to the boundary of the overlap area. By obtaining the weight value used to adjust the cell elevation value in the overlap area, a large range of seamless mosaicking DEM was obtained.

2　Parallel computing strategy

Currently, the improvement in algorithm steps and algorithm performance can improve the efficiency of tie-point extraction to a certain extent; however, improving the efficiency of data processing by reducing the matching accuracy is not desirable. Therefore, based on ensuring the matching accuracy of tie-points, this study also improves the efficiency of tie-point extraction by improving the performance utilisation of hardware. This paper proposes a sliding matching algorithm that combines nested parallel computing of a hybrid CPU and GPU. The multi-threaded CPU is responsible for logical tasks, including data preparation. Parameter setting, video memory allocation, and initialisation, in addition to some tasks with a small amount of computation are also processed by the CPU, whereas the GPU is responsible for processing tasks with a large amount of computation and a high degree of parallelism. The process is illustrated in Fig. 7. This section details the CPU nested parallel computing and GPU parallel computing models.

The tie-points can only be extracted in the overlap area. The CPU processes logical tasks fast. the positions of all overlap areas can be calculated by parallel processing of the multi-threaded CPU. GPU processes image tasks fast. GPU parallel processing is used to extract tie-points in each overlapping area. Hybrid nested GPU parallel computing in each CPU thread of computational overlap area. The images are loaded into GPU global memory. The corresponding standard deviations are calculated to carry out sliding matching, according to the

position division of matching connection points. The coordinates of the images corresponding to the tie-points are calculated. The coordinates of the tie-points are loaded back from GPU global memory.
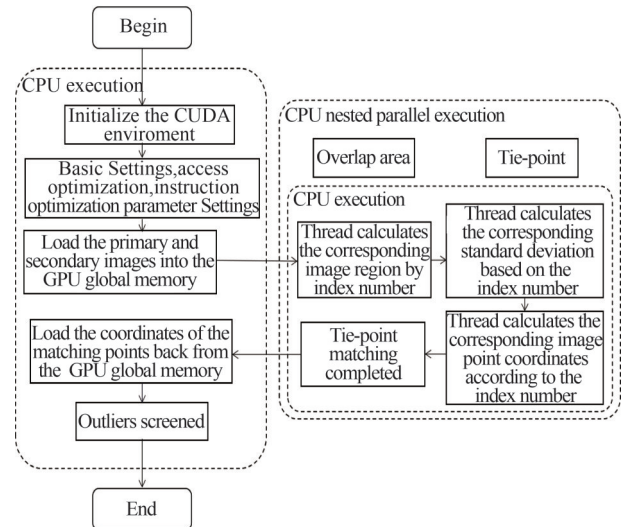
Fig. 7　Collaborative execution process of CPU and GPU after performance optimization
图7　性能优化后CPU和GPU协同执行流程

2.1　CPU nested parallel computing model based on OpenMP

In the CPU parallel computing model, a nested parallel processing algorithm based on the OpenMP compiler is proposed to improve the efficiency of tie-point extraction by simultaneously processing the matching process of multiple tie-points in multiple overlapping regions.

OpenMP uses the fork-join parallel execution mode, which includes the main thread and worker thread. When a thread is already running in a parallel region and comes across another parallel region, a new thread group is generated according to the rules of dynamic threads to execute the nested parallel region. In the process of extracting tie-points, N overlap areas can be separately compiled into N individual tasks using the OpenMP compiler. The compiler produces N worker threads（such as $T1$, $T2$, ⋯, and Tn）, parallel compilation, and thread allocation of the overlap region as shown in Figure 7. When processing each overlap area, the corresponding tie-point pairs of each overlap area can be nested and in parallel to realize the matching of tie-points. M tie-points are compiled into M independent tasks using the OpenMP compiler. The compiler generates M worker threads（such as $T1'$, $T2'$, ⋯, and Tm'）, parallel compilation, and thread allocation of tie-point matching, as shown in Figs. 8-9. When the parallel computation ends, the tie-point extraction process is complete.

2.2　Cuda−based GPU parallel computing model

Among GPU parallel computing models, CUDA is a general-purpose parallel computing architecture from NVIDIA in 2007. It includes a complete solution for GPU computing, which can efficiently accelerate the processing of complex computing on NVIDIA series graphics
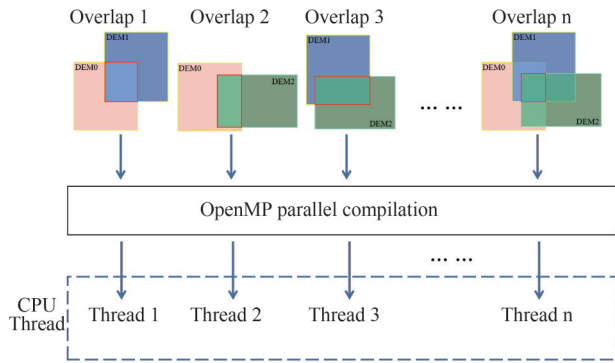
Fig. 8　Flowchart of CPU parallel computing overlap area
图 8　CPU 并行计算重叠区流程图
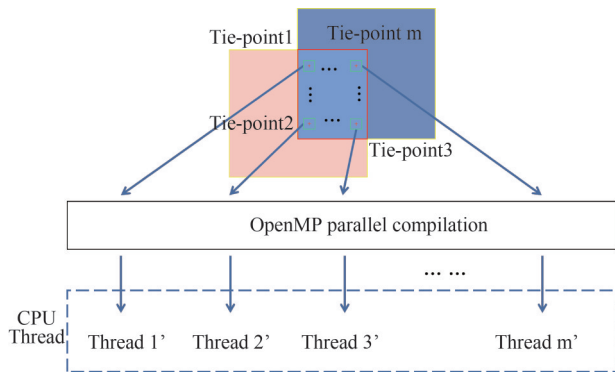
Fig. 9　Tie-point matching flow chart of CPU parallel computing
图 9　CPU 并行计算连接点匹配流程图

cards. A multi-core GPU comprises multiple streaming multiprocessors, each of which comprises multiple streaming processors. During execution, threads are organised into thread blocks and scheduled for execution by a thread block.

In the basic framework structure of the GPU, the parallelism of the tie-point extraction process focuses on the parallelism of the slide matching calculation of the tie-point. The slide matching algorithm of tie-points in the overlapping areas is compiled on CUDA. The matching process of the algorithm is simple to map to the GPU for processing, as shown in Fig. 10. Because the rough matching coordinates and search range of all tie-points have been provided in Sect. 1.1, the sliding matching process of all tie-points is completely independent and parallel, which ensures the computing efficiency of the GPU.

The sliding matching algorithm includes linear interpolation and solving equations of multiple variables; therefore, the parallel computing model of the CPU can also be used to complete the sliding matching operation of the tie-point.

3　Results and discussions

In this section, the experimental results of large-scale and rapid DEM mosaicking are presented, and their accuracy is evaluated. To verify the effectiveness of the DEM mosaicking method, experiments were conducted with the TanDEM-X dataset, and the corresponding
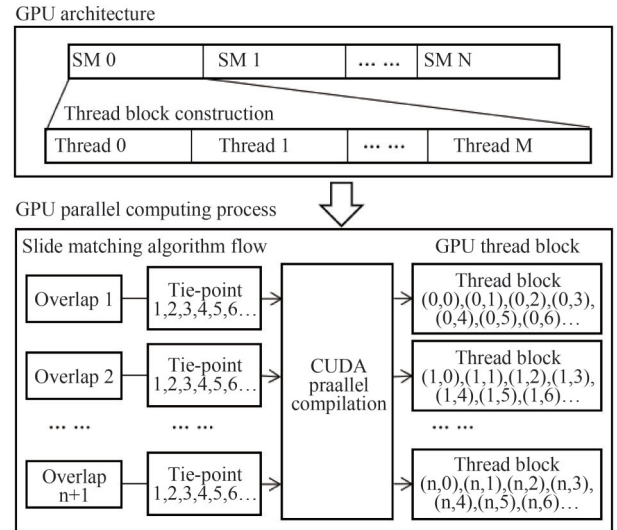
Fig. 10　GPU parallel computing architecture
图 10　GPU 并行计算架构

ICESat laser control points were used as GCPs for DEM block adjustment. Large-scale DEM mosaicking was performed.

The experiment was conducted using c++ 11 compiled on VS2017. The GDAL library was used to process the data and test the complete code on a computer configured with i9-10920xCPU，RTX2080Ti，and 64GB of memory.

3.1　Experimental data
3.1.1　Dataset

The robustness of the proposed method was evaluated. The experimental dataset is listed in Table 2. The orbits of TanDEM-X are ascending. The area of TanDEM spans 110×110 km2 in Zhengzhou City in China and extends approximately $1°30′ \times 1°30′$ from $113°00′$ N latitude and $33°30′$ E longitude. Based on cooperation between the Airbus Defence and Space and German Aerospace Centre, two satellites, TanDEM-X and TerraSAR-X, were developped. They owned synthetic aperture radar that works in the X-band. In the global DEM generated by TanDEM-X, interference data are obtained in the StripMap mode and the reference frame is a WGS84 ellipsoid. **Table 2　Dataset information**

表 2　遥感数据集信息

Dataset	Orbital number	Image umber	Image size （pixels）	Resolution （m）	Terrain
TanDEM−X	4	12	6588×8020	8	plain

The SRTM DEM, based on the C-band InSAR, was developed by a partnership between NASA, NGA and the German and Italian space agencies. Several dataset versions were available. In this study, the latest version of SRTM 4（SRTM DEM4）released by the Space Alliance, distributed in tiles with a spatial resolution of $5° \times 5°$ and available on the CGIAR-CSI website, was used to splice the SRTM into a wide range of DEMs using ENVI

software as a reference DEM for rough matching.

Topographic map of the study area based on the 90m SRTM DEM，as shown in Fig. 11. Solid-lined red box shows the extent of TanDEM for mosaicking. The terrain of the study area is relatively plain.
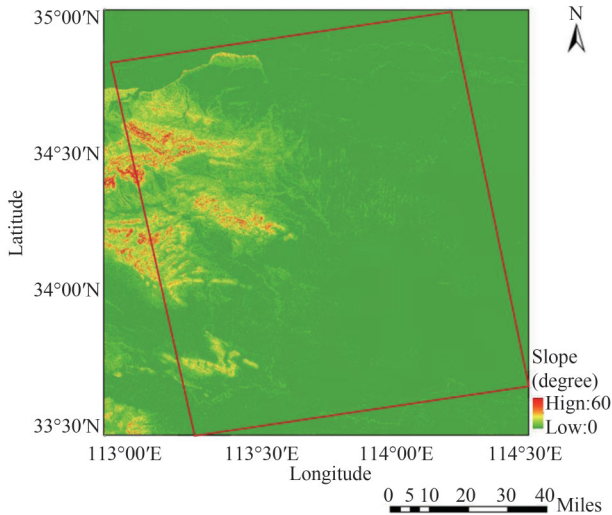
Fig. 11　Slope map of study area.
图11　研究区坡度图

3.1.2　ICESat dataset and control point selection

The ICESat spaceborne laser altimeter data provides the accurate altitude information，classification information and performance evaluation of measuring points distributed around the world[17]. To ensure that the ICESat points used for calibration have good elevation accuracy，multiple selection criteria should be considered，and only the most reliable ones should be extracted[18]. Standards such as surface slope，signal-to-noise ratio，atmospheric conditions，and surface photon ratio are used. Outliers higher than 150 m in comparison to the elevation of the DEM are eliminated. According to previous precision studies，the standard deviations of these corresponding GCPs under optimal conditions are less than 2 m[19]. All the TanDEM-X elevation values within a single ICESat print were averaged，so as to combine the ICESat points with the corresponding DEM pixels[20]. As calibration points for block correction，only uniformly distributed ICESat points in DEM scenes are generally used. Overall，only a portion of the selected ICESat points was used for calibration，using a small number of laser points to verify the final DEM evaluation.

3.2　Experiments

3.2.1　Dense tie-point extraction

Tie-point extraction is the first step in large-scale rapid DEM mosaicking，and its accuracy greatly affects the accuracy of subsequent block adjustment and mosaicking. This study uses the sliding matching method to extract the tie-points，which is different from feature matching method. And sliding matching is the most time-consuming part of tie-point extraction. A total of 401 tie-points pairs were extracted from the TanDEM-X DEM overlaps. Point pairs are shown in green and red，where

the main tie-poinnts of point pairs are shown in red and the tie-points matched are shown in green，（Fig. 12）.
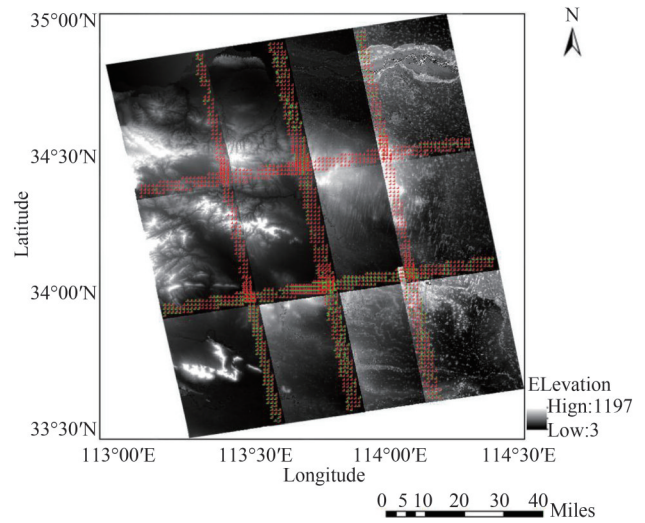
Fig. 12　Distribution of tie-points
图12　连接点分布状况

The CPU/GPU asynchronous parallel method was adopted for the tie-point extraction step. The advantages of CPU/GPU asynchronous parallel were demonstrated by comparing the time consumed with the use or not of CPU/GPU asynchronous parallel，as shown in Table 3. The comparison results show that parallel acceleration improves tie-point extraction efficiency by nearly 18 times.

Table 3　Comparison of parallel acceleration time
表3　并行加速耗时对比

Comparison	Time-consumed /s
Not using parallel acceleration	655.2
Using parallel acceleration	37.59

The corresponding ICESat laser points were obtained based on the TanDEM-X data obtained from InSAR. By setting a grid with a resolution of 20 pixels（160 m），311 uniform high-quality laser elevation control points in the region of interest were obtained. As shown in Fig. 13，the red points represent the corresponding laser elevation control points.

3.2.2　Block adjustment

Combined with the extracted tie-points and laser points，joint block adjustment was performed. The adjustment results were evaluated using 60 ICESat laser check points that were different from the elevation control points. The results are listed in Table 4. This shows that the DEM system error was corrected after the block adjustment.

The root mean square error of the elevation residual between the check points and the DEM decreased considerably，from 3.5 m to 1.1 m. This shows that the DEM systematic error was well corrected by the block adjustment，as shown in Fig. 14.

Resampling after block adjustment is also a time-
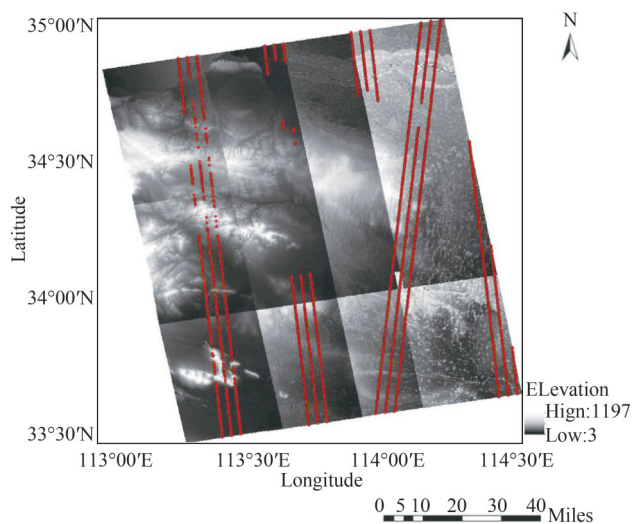
Fig. 13　ICESat laser points（red）superimposed on a TanDEM-X grid image

图 13　ICESat 激光点（红色）叠加在 TanDEM-X 栅格影像中

Table 4　Comparison of check points and digital elevation model（DEM）elevation residuals before and after adjustment

表 4　核检点与 DEM 高程残差平差前后对比

Residuals between check points and DEM elevation	Before block adjustment/m	After block adjustment/m
ABS	23. 613 534	4. 014 245
RMSE	3. 529 182	1. 144 294
MAX	90. 097 908	46. 479 540
MIN	9. 036 408	0. 034 023
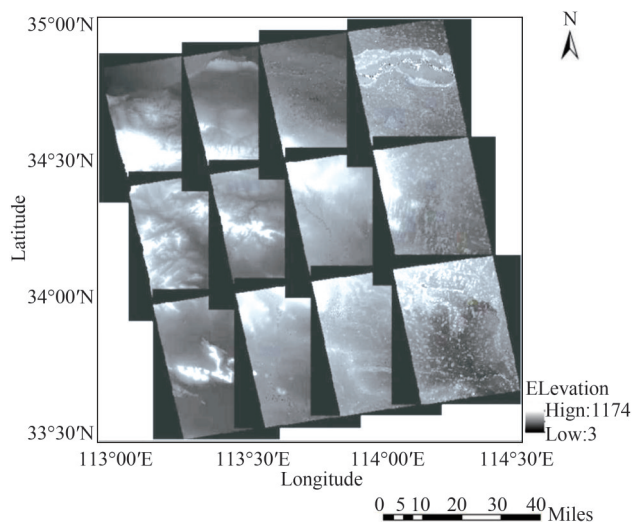
Fig. 14　TanDEM-X grid image after block adjustment

图 14　区域网平差后的 TanDEM-X 栅格影像

consuming step of DEM mosaicking. The efficiency can be greatly improved by CPU parallel computing based on OpenMP，because TanDEM resampling are independent of each other. The results of CPU acceleration are shown in Table 5. And the efficiency of TanDEM resampling is increased by about 9 times.

Table 5　Comparison of resampling parallel acceleration time

表 5　重采样并行加速耗时对比

Comparison	Time-consumed /s
Not using parallel acceleration	163. 7
Using parallel acceleration	18. 5

3. 2. 3　Large-scale DEM mosaicking

The plane and elevation errors in the DEM overlap areas were corrected by a considerable extent after block adjustment. As the difference in the DEM in the along-track direction is smaller than that in the cross-track direction，combined with the feathering-based blend method，the mosaicking strategy of first along-track followed by cross-track was adopted for large-scale DEM mosaicking. The mosaicking results are shown in Fig. 15.
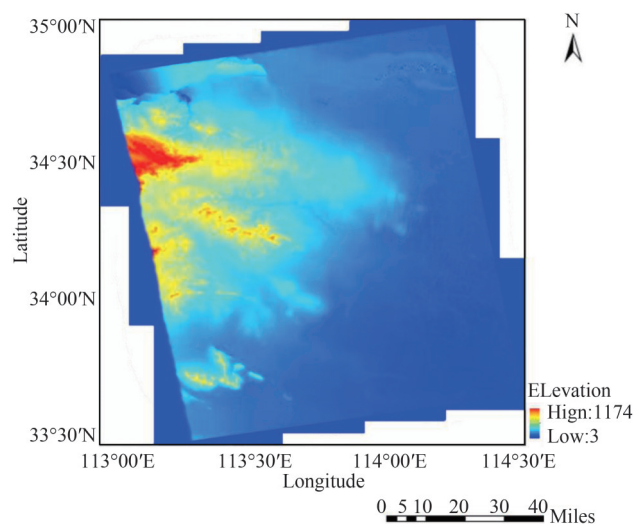
Fig. 15　Large-scale TanDEM-X mosaicking image

图 15　大范围 TanDEM-X 融合影像

4　Conclusions

In this study，a fast DEM mosaicking method was proposed. Dense tie-points were extracted from adjacent DEM overlap areas by allocation of the matching strategy. Combined with the corresponding ICESat elevation control points，block adjustment was performed to estimate the error parameters of the plane and elevation，respectively. Geometric continuity in the plane and elevation directions for TanDEM-X was maintained. A large-scale mosaicking was performed. The experimental results show that the fast DEM mosaicking method created a seamless large-scale multi-stripe DEM mosaicking from the TanDEM-X input DEM scenes. The CPU/GPU parallel acceleration strategy was used to improve the processing efficiency by nearly 18 times.

The executable file of the program available online（https：//github. com/zhhongsh/Fast-Mosaicing-of-InSAR-generated-DEM）.

References

［1］Gesch D B, Muller J P, Farrugia T J. The shuttle radar topography mission – Data validation and applications ［J］. *Photogramm Eng Remote Sens*, 2006, **72**(3):233-235.

［2］Rabus B, Eined Er M, Roth A, *et al*. The Shuttle Radar Topography Mission—A New Class of Digital Elevation Models Acquired by Spaceborne Radar ［J］. *ISPRS J. Photogramm Remote Sens*, 2003, **57**(4):241-262.

［3］Kellndorfer J, Walker W, Pierce L, *et al*. Vegetation height estimation from Shuttle Radar Topography Mission and National Elevation Datasets ［J］. *Remote Sens Environ*, 2004, **93**(3):339-358.

［4］Fu P, Rich P M. A geometric solar radiation model and its applications in agriculture and forestry ［C］. iGISc: Florida, United States, 2000:357-364.

［5］Huang C, Chen Y, Wu J P. Dem-based modification of pixel-swapping algorithm for enhancing floodplain inundation mapping ［J］. *Int J. Remote Sens*, 2014, **35**(1-2):365-381.

［6］WANG Qing-Song. Research on high-efficiency and high-precision processing techniques of spaceborne interferometric synthetic aperture radar［D］. National University of Defense Technology(王青松。星载干涉合成孔径雷达高效高精度处理技术研究。国防科学技术大学), 2011.

［7］YUE Lin-Wei. Research on DEM fusion blending multi-source and multi-scale elevation data［D］. Wuhan University(岳林蔚。多源多尺度DEM数据融合方法与应用研究。武汉大学), 2017.

［8］Huber M, Gruber A, Wessel B, *et al*. Validation of tie-point concepts by the DEM adjustment approach of TanDEM-X［C］. IGARSS: Honolulu Hawaii, United States, 2010:2644-2647.

［9］Gonzalez J H, Antony J M W, Bachmann M, *et al*. Bistatic system and baseline calibration in TanDEM-X to ensure the global digital elevation model quality［J］. *ISPRS J. Photogramm Remote Sens*, 2012, **73**:3-11.

［10］Gruber A, Wessel B, Martone M, *et al*. The TanDEM-X DEM mosaicking: Fusion of multiple acquisitions using InSAR quality parameters［J］. *IEEE J. Sel Topics Appl Earth Observ Remote Sens*, 2016, **9**(3):1047-1057.

［11］Elmiro M, Dutra L V, Mura J C. Calibration of interferometric synthetic aperture radar digital elevation models (DEM) using error surface interpolation methods［C］. WORCAP: Sao Jose Dos Campos, Brazil, 2006.

［12］Jain D S, Rao C V, Kumar S R, *et al*. Assessment of DEM mosaic accuracy［J］. *Int Arch Photogramm Remote Sens*, 2008, **37**(B8): 1137-1141

［13］Kaabouch, Naima, Ghosh, et al. A survey on image mosaicing techniques［J］. *J. Vis. Commun. Image Represent*, 2016, **34**:1-11.

［14］Uss M L, Vozel B, Lukin V V, *et al*. Estimation of Variance and Spatial Correlation Width for Fine-Scale Measurement Error in Digital Elevation Model［J］. *IEEE Trans Geosci Remote Sens*, 2019, **58**(3):1941-1956.

［15］Deng F, Rodgers M, Xie S, *et al*. High-resolution DEM generation from spaceborne and terrestrial remote sensing data for improved volcano hazard assessment—A case study at Nevado del Ruiz, Colombia ［J］. *Remote Sens Environ*, 2019, **233**:111348.

［16］Datla R, Mohan C K, *et al*. A novel framework for seamless mosaic of Cartosat-1 DEM scenes［J］. *Comput Geosci*, 2021, **146**:104619.

［17］Schutz B E, Zwally H J, Shuman C A, *et al*. Overview of the ICESat mission［J］. *Geophys Res Lett*, 2005, **32**(21):L21S01.

［18］Gonzalez J H, Bachmann M, Scheiber R, *et al*. Definition of ICESat selection criteria for their use as height references for TanDEM-X ［J］. *IEEE Trans Geosci Remote Sens*, 2010, **48**(6):2750-2757.

［19］Huber M, Wessel B, Kosmann D, *et al*. Ensuring globally the TanDEM-X height accuracy: Analysis of the reference data sets ICESat, SRTM and KGPS-tracks［C］. IGARSS, Cape Town, South Africa: **2009**:769-772.

［20］Harding D J, Claudia C. ICESat waveform measurements of within-footprint topographic relief and vegetation vertical structure［J］. *Geophys Res Lett*: 2005, **32**(21):L21S10.